Isolation of Mn(I) Compounds Featuring a Reduced Bis(imino)pyridine Chelate and Their Relevance to Electrocatalytic Hydrogen Production

*Tufan K. Mukhopadhyay, Nicholas L. MacLean, Marco Flores, Thomas L. Groy, Ryan J. Trovitch**

School of Molecular Sciences, Arizona State University, Tempe, AZ 85287

ABSTRACT

We report the preparation and electronic structure determination of chelate-reduced Mn(I) compounds that are relevant to electrocatalytic proton reduction mediated by [(^{Ph2PPr}PDI)Mn(CO)][Br]. Reducing [(^{Ph2PPr}PDI)Mn(CO)][Br] with excess Na-Hg afforded a neutral paramagnetic complex, (^{Ph2PPr}PDI)Mn(CO). This compound was found to feature a low spin Mn(I) center and a PDI radical anion as determined by magnetic susceptibility measurement (1.97 μ_B), EPR spectroscopy (S = 1/2), and DFT calculations. When [(^{Ph2PPr}PDI)Mn(CO)][Br] was reduced with K-Hg, Mn(I) complexes with highly-activated CO ligands were obtained. Recrystallization of the reduced product from diethyl ether solution allowed for the isolation of dimeric [(κ^4-^{Ph2PPr}PDI)Mn(μ-η^1,η^2-CO)K(Et_2O)]$_2$ (ν_{CO} = 1710 cm^{-1}, 1656 cm^{-1}), while methyl *tert*-butyl ether treatment afforded dimeric [(κ^4-^{Ph2PPr}PDI)Mn(μ-η^1,η^1-CO)K(MTBE)$_2$]$_2$ (ν_{CO} = 1695 cm^{-1}). Adding 18-crown-6 to these products, or conducting the K-Hg reduction of [(^{Ph2PPr}PDI)Mn(CO)][Br] in presence of 18-crown-6, allowed for the isolation of a monomeric example, (κ^4-^{Ph2PPr}PDI)Mn(μ-η^1,η^2-CO)K(18-crown-6) (ν_{CO} = 1697 cm^{-1}). All three complexes were found to be diamagnetic and were characterized thoroughly by multinuclear 1D and 2D NMR spectroscopy and single crystal X-ray diffraction. Detailed analysis of the metrical parameters and spectroscopic properties suggest that all three compounds possess a Mn(I) center that is supported by a PDI dianion. Importantly, (κ^4-^{Ph2PPr}PDI)Mn(μ-η^1,η^2-CO)K(18-crown-6)

was found to react instantaneously with either $HBF_4 \cdot OEt_2$ or HOTf to evolve H_2 and generate the corresponding Mn(I) complex, [(^{Ph2PPr}PDI)Mn(CO)][BF_4] or [(^{Ph2PPr}PDI)Mn(CO)][OTf], respectively. These products are spectroscopically and electrochemically similar to previously reported [(^{Ph2PPr}PDI)Mn(CO)][Br]. It is believed that the mechanism of [(^{Ph2PPr}PDI)Mn(CO)][Br]-mediated proton reduction involves intermediates that are related to the compounds described herein, and that their ambient temperature isolation is aided by the redox active nature of ^{Ph2PPr}PDI.

INTRODUCTION

Electrocatalytic proton-coupled CO_2 reduction has emerged[1-4] as a reaction of interest since CO can be converted into liquid fuels using the Fischer-Tropsch process. Recently, group 7 transition metal electrocatalysts for the conversion of CO_2 to CO have been shown to operate at low overpotentials with high turnover number (TON) and Faradaic efficiency.[5-20] The electrocatalytic reduction of H^+ sources to evolve H_2 (which is a competing reaction in proton-coupled CO_2 reduction) represents another transformation that converts stored energy into fuel.[1] While there are several known Mn electrocatalysts for CO_2 reduction,[5-10,13,14] only a few have been shown to reduce H^+ electrochemically.[21-27] The first monomeric Mn-based H^+ reduction electrocatalysts were reported by Valyaev *et al.,* where Mn vinylidene and allenylidene complexes were found to reduce the protons of HBF_4 at -1.60 V and -0.84 V vs. $Fc^{+/0}$ in MeCN, respectively.[22] In 2014, Fan and co-workers[23] described a dimanganese hexacarbonyl complex possessing bridged sulfide ligands that catalyzes H_2 evolution from trifluoroacetic acid with impressive activity at -1.50 V vs. $Fc^{+/0}$ (0.69 V overpotential according to the methods described by Appel and Helm[28]). The same group subsequently reported a 1,2-benzenedithiol-derived variant that reduces the protons of acetic acid at -2.10 V vs. $Fc^{+/0}$,[24] and dimeric Mn complexes with selenide linkages that require higher overpotentials than their sulfide counterparts.[25] Shortly thereafter, Kubiak and co-workers demonstrated that [Mn(mesbpy)$(CO)_3$(MeCN)][OTf] can electrochemically reduce protons at -1.55 V vs. $Fc^{+/0}$ using trifluoroacetic acid.[26] The efficiency of this compound and related group 7 metal electrocatalysts for CO_2 reduction has been linked to the redox activity of bipyridine,[10,29] which serves to stabilize [(bpy)Mn$(CO)_3$]$^-$ intermediates that feature a reduced chelate.[30,31]

Like bipyridine, bis(imino)pyridine (or pyridine diimine, PDI) ligands are well-known to accept electrons from low-valent first row transition metals,[32,33] rendering them a promising

supporting scaffold for Mn-based electrocatalysis. In 1994, it was demonstrated that refluxing ^{iPr2Ar}PDI in the presence of $(CO)_5MnBr$ results in the displacement of three CO ligands and the formation of (^{iPr2Ar}PDI)Mn(CO_2)Br.[34] In 2015, our group reported that addition of the phosphine-substituted ligand ^{Ph2PPr}PDI[35] to $(CO)_5MnBr$ results in the loss of five CO ligands and displacement of bromide anion from the metal coordination sphere to generate [(^{Ph2PPr}PDI)Mn(CO)][Br] (**1**) (eq 1).[27] In this report, we showed that **1** undergoes a reversible 2e$^-$ reduction at -1.92 V vs $Fc^{+/0}$. An increase of current density to 2.1 mA/cm^2 (i_{cat}/i_p = 4.2) was observed when this catalyst was added to a CO_2-saturated MeCN solution containing 1.05 M MeOH. Controlled potential coulometry revealed that **1** produces H_2 with 96.7% Faradaic efficiency as a result of CO_2 acidification (pseudo pH = 8.4, for control experiments see reference 27). Herein, we present the isolation and electronic structure evaluation of compounds that are relevant to the mechanism of **1**-mediated H_2 evolution.

RESULTS AND DISCUSSION:

Synthesis and Characterization: Knowing that the cyclic voltammogram of **1** displays a 2e$^-$ reversible wave at -1.92 V vs $Fc^{+/0}$, chemical reduction of **1** was sought to isolate reduced Mn species relevant to electrocatalytic H_2 production. Reduction of **1** with excess Na-Hg in THF for 6 h yielded a paramagnetic complex exhibiting broadened ^{1}H NMR resonances over a narrow range (from 5-11 ppm), suggesting the formation of (^{Ph2PPr}PDI)Mn(CO) (**2**) (eq 1). In KBr, the infrared spectrum of **2** featured a CO stretching frequency at 1782 cm^{-1}, representing a 43 cm^{-1} shift to lower energy from **1** (1825 cm^{-1}).[27] The UV-Vis spectrum of **2** shows three intense absorptions at 335 nm (ε = 17600 M^{-1}cm^{-1}), 395 nm (ε = 14000 M^{-1}cm^{-1}) and 538 nm (ε = 14400 M^{-1}cm^{-1}) and a weaker absorption at 674 nm (ε = 4000 M^{-1}cm^{-1}) (Figure S44, Table S1). Cooling a concentrated toluene solution of **2** layered with diethyl ether furnished purple crystals suitable for X-ray diffraction. The solid-state structure of **2** (Figure 1) was found to exhibit a distorted octahedral geometry with significant PDI reduction, as evident from the elongated C(2)-N(1) and C(8)-N(3) bond distances [1.360(4) and 1.349(4) Å, respectively, Table 1] and contracted C(2)-C(3) and C(7)-C(8) bond lengths [1.427(5) Å each].[32,33] Also, the short Mn-N distances (Table 1) are consistent with the sum of the covalent radii of N and a low-spin Mn center.[36] Notably, the

increase in CO bond length from 1.177(7) Å in **1**[27] to 1.192(4) Å with concomitant shortening of Mn(1)-C(40) from 1.773(7) Å in **1** to 1.757(3) Å suggest additional backbonding.

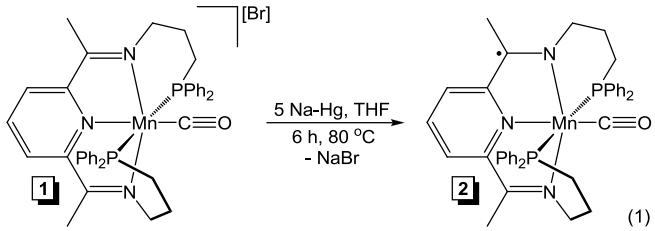

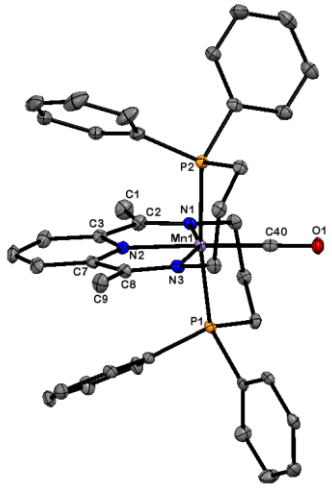

Figure 1. Solid state structure of **2** shown at 30% probability ellipsoids. Hydrogen atoms are omitted for clarity. Selected bond lengths and angles are given in Table 1.

Table 1. Bond lengths (Å) and angles (˚) determined for **2**, **3-Et₂O**, **3-MTBE**, and **4**.

	2	**3-Et₂O**	**3-MTBE**	**4**
Mn(1)-N(1)	1.991(3)	1.929(7)	1.925(4)	1.9352(17)
Mn(1)-N(2)	1.950(3)	1.869(7)	1.885(4)	1.8844(16)
Mn(1)-N(3)	1.984(3)	1.940(7)	1.931(4)	1.9418(16)
Mn(1)-C(40)	1.757(3)	1.747(11)	1.749(5)	1.754(2)
N(1)-C(2)	1.360(4)	1.355(11)	1.366(6)	1.357(3)
N(3)-C(8)	1.349(4)	1.368(11)	1.345(6)	1.357(3)
C(2)-C(3)	1.427(5)	1.406(13)	1.394(7)	1.404(3)
C(7)-C(8)	1.427(5)	1.405(12)	1.409(7)	1.412(3)
C(40)-O(1)	1.192(4)	1.196(11)	1.194(6)	1.200(2)
P(1)-Mn(1)-P(2)	173.02(4)	-	-	-
N(1)-Mn(1)-N(3)	156.04(11)	157.5(3)	157.72(17)	157.38(7)
P(1)-Mn(1)-N(2)	92.23(8)	131.9(2)	121.82(12)	120.43(5)
N(2)-Mn(1)-C(40)	178.20(14)	137.4(4)	151.5(2)	150.61(8)
N(1)-Mn(1)-P(1)	80.83(8)	92.1(3)	88.56(12)	88.70(5)

The solution state magnetic susceptibility of **2** was found to be 1.97 μ_B (296 K), which suggests the presence of one unpaired electron. To determine whether this electron resides on Mn or in one of the PDI LUMOs, a toluene solution of **2** was prepared and analyzed by X-band electron paramagnetic resonance (EPR) spectroscopy at 296 and 120 K (Figure 2). The EPR signal observed at 296 K (liquid solution) is centered near a *g*-value of 2.0 indicating that it belongs to a single spin center (S = ½) (Figure 2A). In addition, the signal shows two different splitting patterns, one is a three-line splitting with intensities in the ratio of 1:2:1 and the other is a two-line splitting, resulting in a total of six lines. These spectral features are due to the hyperfine coupling (hfc) interactions between the magnetic moment of the unpaired electron and the magnetic moments of three ^{1}H (I = ½) nuclei from the pyridine ring of ^{Ph2PPr}PDI, with two of them being equivalent. The EPR signal observed at 120 K (frozen solution) is slightly broader than the one observed at 296 K (Figure 2B) indicating that the anisotropies, corresponding to the *g*-values ($\boldsymbol{g}$) and hfc interactions ($\boldsymbol{A}^{H_i}$ and $\boldsymbol{A}^{H_3}$), are rather small.

Thus, the EPR spectrum of **2** at 296 K was well-fit (σ = 1.2 %, see Experimental section) considering a single spin center (S = ½) with an isotropic *g* value of 1.995 and isotropic hfc's of 183 MHz and 78 MHz (see Figure 2A and Table 2). This finding is consistent with the crystallographically-determined structure of **2** which shows three pyridine hydrogen atoms, two of them being symmetrically related within the ^{Ph2PPr}PDI ligand (Figure 1). The principal components of the $\boldsymbol{g}$, $\boldsymbol{A}^{H_i}$ and $\boldsymbol{A}^{H_3}$ tensors were obtained via simulation of the EPR spectrum observed at 120 K (see Figure 2B and Table 2). Furthermore, the observed isotropic hfc's indicate that the central pyridine of **2** carries a large fraction of the electron spin distribution.

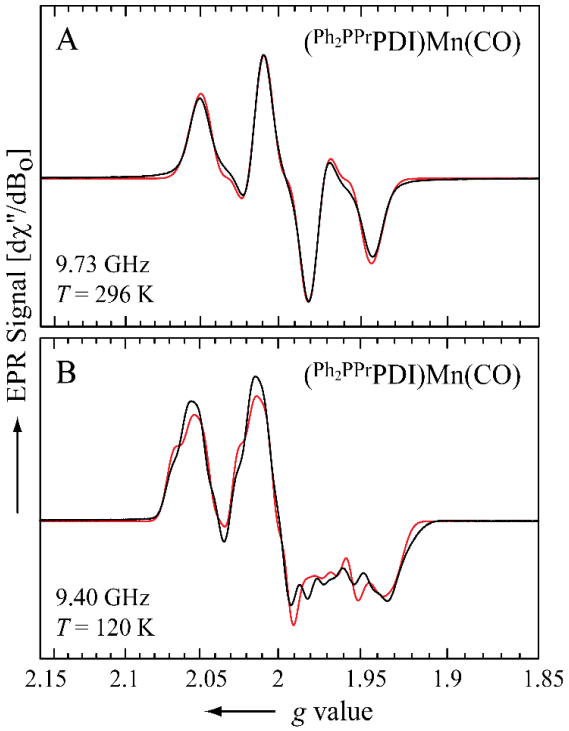

Figure 2. Experimental (black) and simulated (red) X-band EPR spectra of **2** in toluene at 296 K (liquid solution) (A) and at 120 K (frozen solution) (B). The EPR spectrum at 296 K shows two different splitting patterns. These were attributed to the hyperfine couplings between the unpaired electron and three protons, with two of them being equivalent (see text).

Table 2. Parameters used to fit the EPR spectra of **2** at 120 and 296 K.

Parameter[a]	T = 120 K	T = 296 K
g_x	2.021	
g_y	1.998	
g_z	1.971	
g_{iso}		1.995
$\lvert A_x^{H_i}\rvert$	184 MHz	
$\lvert A_y^{H_i}\rvert$	184 MHz	
$\lvert A_z^{H_i}\rvert$	184 MHz	
$\lvert A_{iso}^{H_i}\rvert$		183 MHz
$\lvert A_x^{H_3}\rvert$	51 MHz	
$\lvert A_y^{H_3}\rvert$	42 MHz	
$\lvert A_z^{H_3}\rvert$	44 MHz	
$\lvert A_{iso}^{H_3}\rvert$		78 MHz

[a]See the Experimental Section for the definition of the fitting parameters. Errors for g_x, g_y, g_z, and g_{iso} are ±0.001. Errors for $A_x^{H_i}$, $A_y^{H_i}$, $A_z^{H_i}$, $A_{iso}^{H_i}$, $A_x^{H_3}$, $A_y^{H_3}$, $A_z^{H_3}$, and $A_{iso}^{H_3}$ are ±1 MHz.

Taken together, the metrical parameters and EPR results suggest that **2** is best described as a low-spin Mn(I) complex that features a PDI radical monoanion. To further support this electronic structure determination, DFT calculations were performed. The geometry was optimized using the PBE functional and 6-31g(d, p) basis set for all atoms. The bond distances and angles obtained closely match those observed experimentally (Table S2). Therefore, single point energy calculations on the optimized geometry were conducted using the PBE functional. The frontier molecular orbitals were found to contain a SOMO featuring electron density that is delocalized throughout the PDI chelate backbone (only 4% Mn character observed, see Figure S45). In contrast, the doubly-occupied d_{xy}, d_{xz}, and d_{yz} orbitals were found to have significant Mn character (52-63%). A single point energy calculation on the crystal structure geometry was also performed using the B3LYP functional and similar orbital population was obtained. The EPR data and DFT results strongly indicate the presence of a delocalized PDI-based electron. Notably, the broadened ^{1}H NMR resonances exhibited by **1** are observed near the diamagnetic region, which is also suggestive of ligand-based paramagnetism.

When **1** was reduced with excess K-Hg, a diamagnetic complex was isolated after 12 h (eq 2), which shows two different ^{31}P NMR signals at 82.07 and -16.37 ppm, indicative of a κ^4-*P*,*N*,*N*,*N*-PDI chelate. Dark green crystals of this product were obtained by cooling a concentrated diethyl ether solution to -35 °C and analysis by single crystal X-ray diffraction revealed dimeric $[(\kappa^4\text{-}^{Ph2PPr}PDI)Mn(\mu\text{-}\eta^1,\eta^1,\eta^2\text{-}CO)K(Et_2O)]_2$ (**3-Et$_2$O**) (Figure S49), albeit with poor data quality (R_1 = 0.0998, see Table S7). The solid-state structure of **3-Et$_2$O** exhibits a significantly reduced PDI chelate as judged by the elongated C(2)-N(1) and C(8)-N(3) distances and contracted C(2)-C(3) and C(7)-C(8) distances listed in Table 1. Notably, weak end-on interactions were observed between the CO ligand and K^+ ion, which was also found to interact with the CO ligand of the adjacent molecule in a side-on fashion. Additionally, each K^+ ion features weak interactions to one chelate PPh_2 substituent, one diethyl ether molecule, and the π-system of ^{Ph2PPr}PDI (Figure S49).

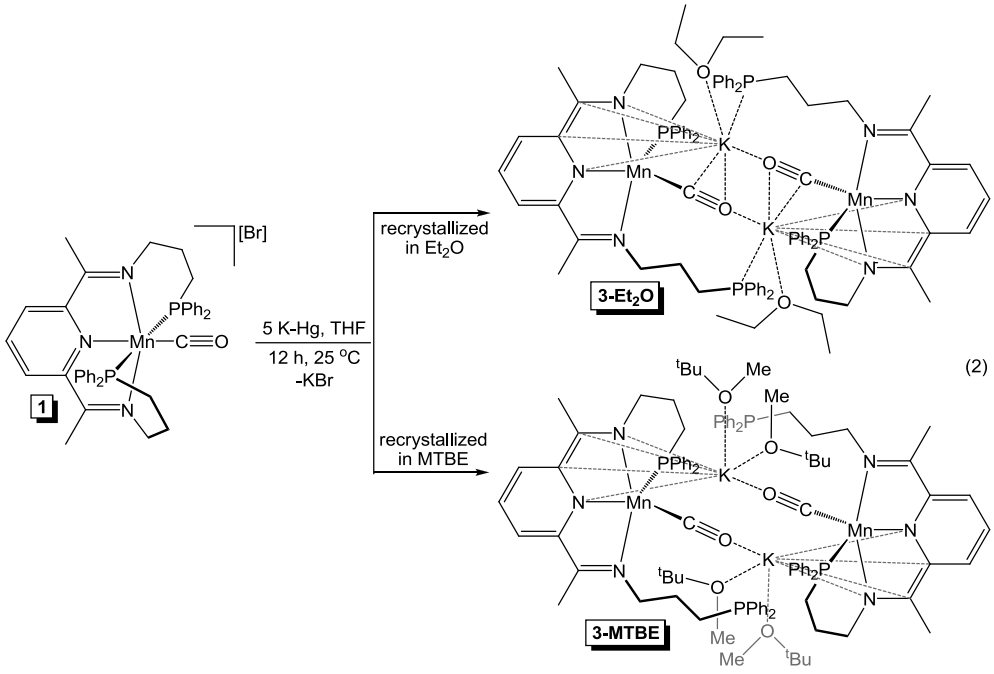

The structure and composition of **3-Et₂O** were confirmed by ^{1}H, ^{13}C, gCOSY, and gHSQCAD NMR spectroscopy (Figure S3-S7) and elemental analysis. Two ^{1}H NMR singlets at 2.80 and 2.65 ppm indicate the presence of inequivalent PDI methyl groups while the doublets observed at 8.05 and 7.94 ppm are consistent with two *meta*-pyridine positions and a tetradentate ^{Ph2PPr}PDI chelate. One coordinated diethyl ether molecule per monomeric unit was observed at 3.25 and 1.10 ppm. Due to side-on, end-on carbonyl coordination to potassium, the infrared spectrum of **3-Et₂O** appears to show two CO stretching frequencies at 1710 and 1656 cm^{-1}, which are of considerably lower energy than the carbonyl stretch of **2**. A search of the literature revealed one comparable cobalt monocarbonyl compound that is bridged through potassium in an η^1,η^2-fashion (ν_{CO} = 1690 cm^{-1})[37] and a handful of iron dicarbonyl examples featuring related bonding modes.[38-40] A comparison of CO stretching frequencies for each compound prepared in this study is illustrated in Figure 3.

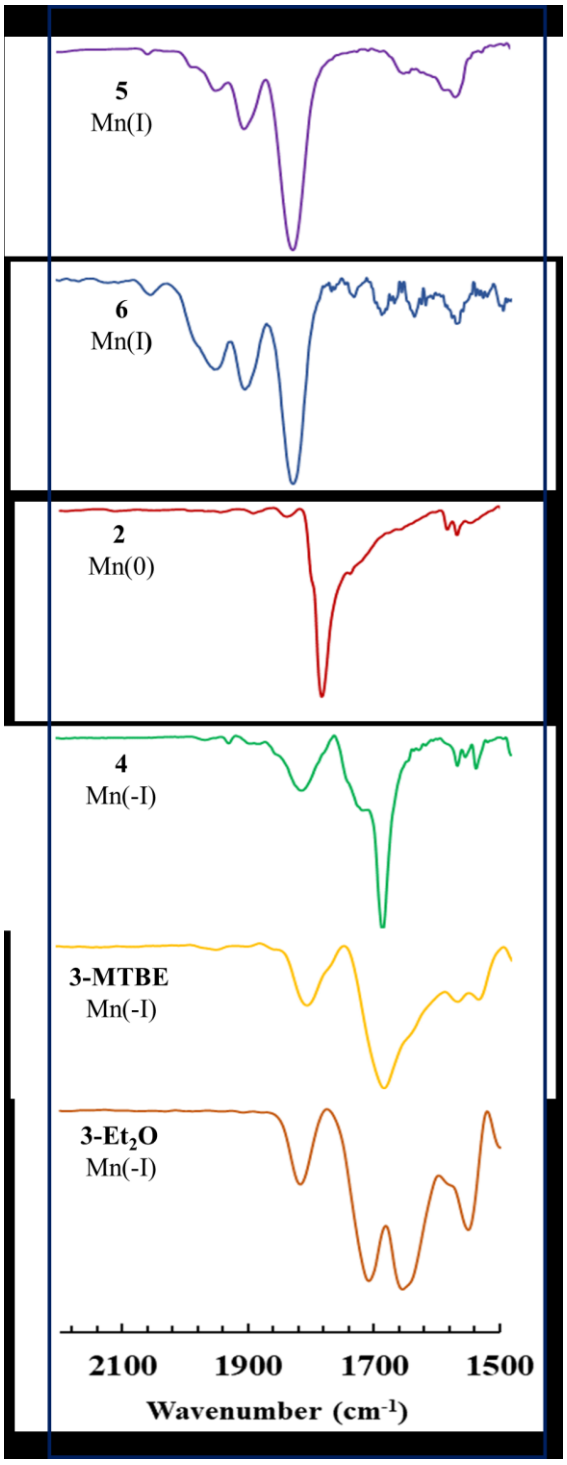

Figure 3. Abridged infrared spectra showing the CO stretching frequencies of **2** (red, 1782 cm^{-1}), **3-Et$_2$O** (orange, 1710 and 1656 cm^{-1}), **3-MTBE** (yellow, 1695 cm^{-1}), **4** (green, 1697 cm^{-1}), **5** (purple, 1834 cm^{-1}), **6** (blue, 1834 cm^{-1}). To highlight differences in metal-to-carbonyl backbonding, the formal oxidation state of Mn is provided (i.e., the oxidation state determined from the formal oxidation state method of electron counting, which assumes a neutral ^{Ph2PPr}PDI chelate).

In an attempt to improve upon crystal quality, the compound was recrystallized from methyl *tert*-butyl ether (MTBE) and a similar dimeric structure [(κ^4-^{Ph2PPr}PDI)Mn(μ-η^1,η^1-CO)K(MTBE)$_2$]$_2$ (**3-MTBE**, eq 2) was observed. This complex is diamagnetic and complete structural analysis was performed using 1D and 2D NMR spectroscopy (Figure S9-S14). Two ^{31}P resonances were located at 82.79 (coordinated to Mn) and -15.69 (free) ppm, indicating κ^4-*P*,*N*,*N*,*N*-PDI coordination. Like **3-Et$_2$O**, **3-MTBE** displays two different singlets for the PDI methyl groups (2.80 and 2.64 ppm) and two doublets for the *meta*-pyridine protons (8.06 and 7.64 ppm), owing to the absence of C_2 symmetry. Although the solid-state structure has two MTBE molecules coordinated to each K^+ ion, integration of the ^{1}H NMR spectrum showed that only one remains attached in solution. In both **3-Et$_2$O** and **3-MTBE**, the Mn center was found to possess a distorted trigonal bipyramidal geometry (Figures S48-S49). For **3-MTBE**, the CO ligand is bound to K^+ in an η^1-fashion through oxygen, and IR spectroscopy again revealed an unusually low CO stretching frequency of 1695 cm^{-1}. The PDI chelate in **3-MTBE** is highly reduced as evident from the elongated C(2)-N(1) and C(8)-N(3) bonds [1.366(6) and 1.345(6) Å, respectively] and contracted C(2)-C(3) and C(7)-C(8) bonds [1.394(7) and 1.409(7) Å, respectively].[32,33] The shorter Mn(1)-C(40) bond length of 1.749(5) Å (relative to 1.773(7) Å in **1** and 1.757(3) Å in **2**) indicates increased back donation.

Although the core atom positions were accurately determined, the crystal structure of **3-MTBE** features disordered *tert*-butyl groups, causing the data to not fall under the required publication quality limit (R_1 = 0.1060, see Table S7). Therefore, the same reduction was conducted in the presence of one equivalent of 18-crown-6 in order to isolate a monomeric formal Mn(-I) complex. Indeed, a diamagnetic complex (κ^4-^{Ph2PPr}PDI)Mn(μ-η^1,η^2-CO)K(18-crown-6) was isolated (eq 3, **4**), which exhibits two ^{31}P NMR singlet resonances at 86.27 (coordinated to Mn) and -15.69 ppm (free), indicating κ^4-*P,N,N,N*-PDI coordination. Similarly, a non-C_2-symmetric structure was confirmed upon observing unique PDI methyl and *meta*-pyridine signals in the ^{1}H NMR spectrum. The 18-crown-6 ligand was observed as a singlet at 2.90 ppm. The IR spectrum of this compound was found to feature a CO stretching frequency at 1697 cm^{-1}, which is 85 cm^{-1} lower than that of **2**. Compound **4** was also obtained quantitatively when isolated **3-Et$_2$O** or **3-MTBE** was treated with two equivalents of 18-crown-6.

Single crystals of **4** suitable for X-ray diffraction were obtained by cooling a concentrated diethyl ether solution layered with pentane. The solid-state structure (Figure 4) was found to

feature a monomeric Mn complex possessing a distorted square pyramidal geometry as evident from the N(2)-Mn(1)-C(40), P(1)-Mn(1)-C(40), and N(2)-Mn(1)-P(1) angles of 150.61(8)˚, 88.30(7)˚, and 120.43(6)˚ respectively. The PDI fragment is reduced by two electons,[32,33] resulting in elongation of the N(1)-C(2) and N(3)-C(8) bonds with concomitant shortening of the C(2)-C(3) and C(7)-C(8) bonds (Table 1). Backbonding to the CO ligand is also increased, as indicated by the elongated C(40)-O(1) bond [1.200(2) Å] and contracted Mn(1)-C(40) bond [1.754(2) Å].

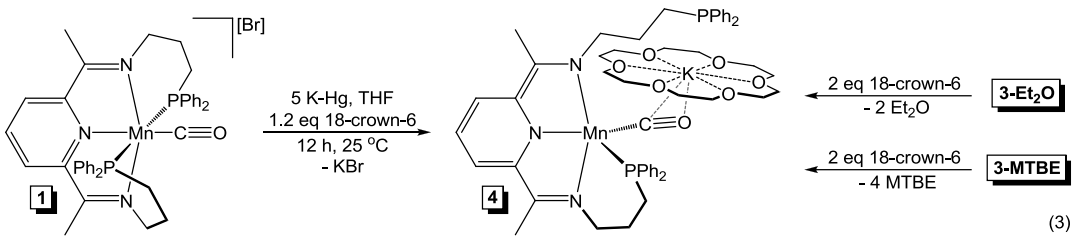

(3)

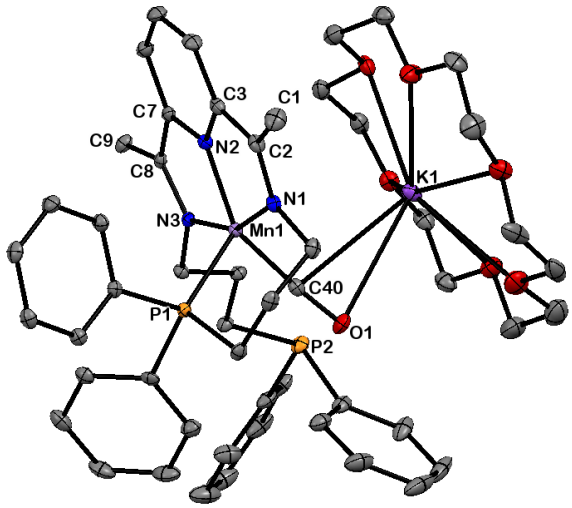

Figure 4. Solid state structure of **4** shown at 30% probability ellipsoids. Hydrogen atoms are omitted for clarity. One O-atom in the 18-crown-6 is positionally disordered and omitted for clarity. Selected bond lengths and angles are given in Table 1.

It should be noted that **3-Et2O**, **3-MTBE**, and **4** have average C(2)-N(1) and C(8)-N(3) distances of 1.359 and 1.357 Å and average C(2)-C(3) and C(7)-C(8) distances of 1.401 and 1.409 Å, respectively, which resemble the reported values for a doubly reduced PDI ligand.[32,33] Considerable ligand reduction is also reflected in the unusually low CO stretching frequencies

observed for **3-Et$_2$O** (1710, 1656 cm^{-1}), **3-MTBE** (1695 cm^{-1}), and **4** (1697 cm^{-1}, Figure 3). For comparison, the CO stretches reported by Kubiak and co-workers for [Mn(mesbpy)(CO)$_3$][K(18-crown-6)] were located at 1917 and 1815 cm^{-1} in THF solution.[10] The electronic absorption spectra of **3-Et$_2$O** and **3-MTBE** were found to exhibit high energy charge transfer bands with molar absorptivity values between 20,000-60,000 M^{-1}cm^{-1} (bands of similar energy were observed for **2** and **4**, but were found to have lower extinction coefficients of between 10,000-20,000 M^{-1}cm^{-1}, see Figure S44). Considering our experimental observations and the electronic structure descriptions of previously reported (^{Ph2PPr}PDI)MnH[41] and [Na(OEt$_2$)$_3$][(^{iPr2Ar}PDI)Mn(CO)$_2$][42] it can be proposed that **3-Et$_2$O**, **3-MTBE**, and **4** possess low-spin Mn(I) centers that are supported by singlet PDI dianions (as indicated in eq 2 and 3). To further support this assignment, a single point energy calculation was conducted on the crystallographically determined atom positions of **4** using the PBE functional. The two highest occupied molecular orbitals were found to possess π-bonding character between d_{yz} and the C_2-symmetric π* orbital of ^{Ph2PPr}PDI[41] (Figure S46). This mixing indicates that both orbitals are doubly-occupied and that the ^{Ph2PPr}PDI-based electrons are paired. Ultimately, the redox active nature of ^{Ph2PPr}PDI is crucial for enabling the isolation of **3-Et$_2$O**, **3-MTBE**, and **4** at ambient temperature.

Given the reversible nature of the 2e$^-$ reduction wave in the cyclic voltammogram of **1**,[27] it is believed that **3-Et$_2$O, 3-MTBE**, and **4** are structurally analogous to the active species responsible for **1**-mediated proton reduction. The previously mentioned, 5-coordinate bipyridine complex [Mn(mesbpy)(CO)$_3$][K(18-crown-6)] was proposed to be the active intermediate for electrocatalytic CO_2 reduction,[10] and evaluating the properties and reactivity of such compounds is important for developing improved Mn electrocatalysts. To better understand the proton reduction mechanism using **1**, the reactivity of **4** was evaluated due to its monomeric nature, simple spectroscopic identification, and high-yielding synthesis. When two equivalents of CF_3SO_3H were added to a THF solution of **4**, a bright purple diamagnetic complex identified as [(^{Ph2PPr}PDI)Mn(CO)][OTf] (**5**) formed instantaneously (eq 4). The ^{31}P NMR spectrum of **5** showed a singlet at 53.79 ppm, which is similar to the shift reported for **1** (55.42 ppm).[27] The triflate counter anion was observed by ^{19}F NMR spectroscopy as a singlet at -79.30 ppm (Figure S31) and the structure was further verified by ^{13}C and 2D NMR analysis (Figure S24-S29). The CO stretching frequency of **5** was observed at 1834 cm^{-1} (Figure 3), which is close to the value

reported for **1** (1825 cm^{-1}, KBr).[27] A cyclic voltammogram of **5** was obtained (Figure 5) and was found to exhibit two reversible waves at -0.29 V (vs $Fc^{+/0}$) and -1.92 V (vs $Fc^{+/0}$), analogous to the waves observed for **1**.

Similarly, adding two equivalents of $HBF_4 \cdot OEt_2$ to a THF solution of **4** resulted in the immediate formation of a purple compound identified as [(^{Ph2PPr}PDI)Mn(CO)][BF_4] (**6**, eq 4), which exhibits a similar ^{31}P NMR spectrum (a single resonance at 55.84 ppm). The BF_4 anion shows a broad resonance at -151.78 ppm in the ^{19}F NMR spectrum and a sharp singlet at -2.45 ppm in the ^{11}B NMR spectrum (Figures S39-S40). The infrared spectrum of **6** features a CO stretching frequency at 1834 cm^{-1} and the cyclic voltammogram of this complex possesses two reversible waves at -0.28 V and -1.92 V vs $Fc^{+/0}$ (Figure S43). Both **5** and **6** display relatively weak UV-visible charge transfer bands that have extinction coefficients between 1,000-5,000 $M^{-1}cm^{-1}$ (Figure S44, Table S1). Comparing the cyclic voltammograms, NMR spectra, CO stretching frequencies, and electronic absorption spectra of **5** and **6** to the corresponding values reported for **1**, it is reasonable to propose that all three complexes possess a Mn(I) center that is supported by a neutral PDI.[27] Complexes **5** and **6** were also prepared directly by treating **1** with either $AgBF_4$ or AgOTf, respectively (eq 4, right).

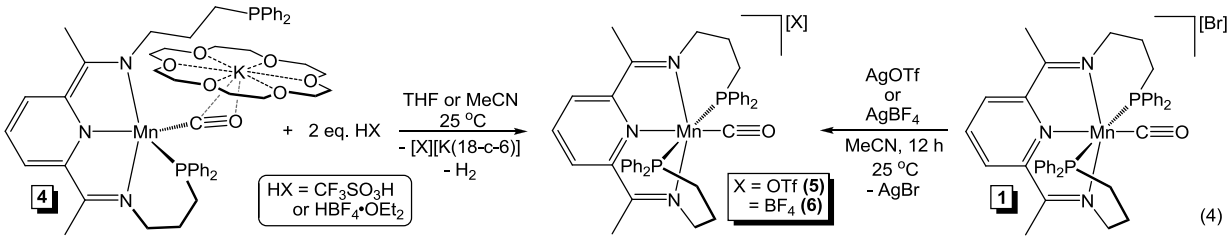

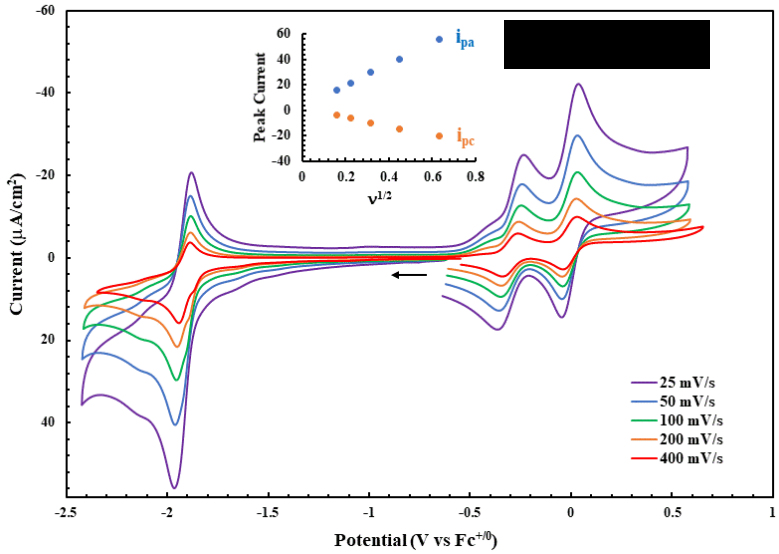

Figure 5. Cyclic voltammograms of **5** in 0.1 M $TBAPF_6$/MeCN. Ferrocene was used as internal standard (wave centered at 0.0 V). Potential scan rate is varied. The arrow indicates the direction of cycling. In the inset, the linear relation of peak current and square root of scan rate is shown (Randles-Sevcik equation) for the wave at -1.94 V.

According to the proton reduction mechanism proposed by Fan and coworkers,[25] a reduced dimeric Mn complex reacts with H^+ to form a hydride species, which then reacts with a second equivalent of H^+ to release H_2 and regenerate the catalyst. To probe the mechanism of **1**-mediated proton reduction, two equivalents of $HBF_4 \cdot OEt_2$ were added to a frozen acetonitrile-d_3 solution of **4** in a J. Young tube and capped immediately. Warming up to ambient temperature resulted in an instantaneous color change from brownish-green to bright purple. Analysis by ^1H NMR spectroscopy revealed a singlet at 4.51 ppm that is consistent with H_2 formation (this peak disappeared after evacuating the headspace of the tube, see Figure S42). Efforts to observe a catalytic intermediate in this fashion were unsuccessful and attempts to add a single equivalent of HBF_4 resulted in partial conversion of **4** to **6**. Likewise, adding $NaEt_3BH$ to **1** or **6** did not allow for observation of a neutral Mn(I) hydride complex and no reaction was observed upon adding 1 atm H_2 to **4**. It is believed that **4** reacts with one equivalent of HBF_4 to generate a short-lived Mn(I) hydride intermediate, possible isomers of which are shown in eq 5. Considering the electronic structure of **4**, this step involves the transfer of two ligand-based electrons into the newly formed Mn-H bond. This intermediate hydride species quickly releases H_2 upon reacting with a second equivalent of HBF_4 to generate **6**. When reducing potentials are applied, cationic

species such as **1**, **5**, and **6** can be reduced by two electrons to regenerate electrocatalytically relevant Mn complexes featuring a doubly reduced ^{Ph2PPr}PDI chelate that are analogous to **4**.

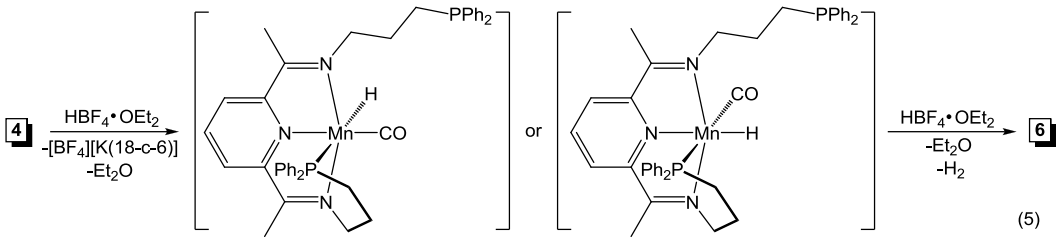

CONCLUSION

We have prepared several low-valent Mn compounds by exploring the chemical reduction of [(^{Ph2PPr}PDI)Mn(CO)][Br], which was previously reported to mediate electrocatalytic hydrogen evolution. Detailed electronic structure analysis using multinuclear NMR spectroscopy and single crystal X-ray diffraction has revealed that the Mn(I) oxidation state is maintained throughout reduction as electrons are added to the ^{Ph2PPr}PDI chelate. Notably, the products possessing a doubly-reduced ^{Ph2PPr}PDI chelate were found to feature significantly weakened CO ligands relative to other low-valent Mn carbonyl complexes. It has also been discovered that the addition of proton sources to (κ^4-^{Ph2PPr}PDI)Mn(μ-η^1,η^2-CO)K(18-crown-6) allows for utilization of these ligand-based electrons, the evolution of H_2, and generation of the respective Mn(I) cation, offering insight into the mechanism of [(^{Ph2PPr}PDI)Mn(CO)][Br]-mediated electrocatalytic proton reduction.

EXPERIMENTAL SECTION**:**

General Considerations: All synthetic manipulations were conducted in an MBraun glovebox under an atmosphere of purified nitrogen. Anhydrous solvents were purified using a Pure Process Technology solvent system and stored in the glovebox over activated 4 Å molecular sieves and sodium before use. Acetonitrile and *tert*-butyl methyl ether were sourced from Sigma-Aldrich, dried by distillation, and stored over 3 Å or 4 Å molecular sieves, respectively. Benzene-d_6 and acetonitrile-d_3 were purchased from Oakwood Chemicals and acetone-d_6 was purchased from Cambridge Isotope Laboratories. All NMR solvents were dried over 4 Å molecular sieves before use, with the exception of acetonitrile-d_3 which was dried over 3 Å molecular sieves.

Trifluoromethanesulfonic acid and $(CO)_5MnBr$ were used as received from Strem Chemicals. Lutidine was purchased from Acros Organics and $HBF_4 \cdot OEt_2$ was obtained from Sigma-Aldrich. [(^{Ph2PPr}PDI)Mn(CO)][Br] (**1**) was prepared according to the published procedure.[27]

Solution ^{1}H nuclear magnetic resonance (NMR) spectra were recorded at room temperature on a Varian 500-MR NMR spectrometer. All ^{1}H and ^{13}C NMR chemical shifts (ppm) are reported relative to $Si(CH_3)_4$ using ^{1}H (residual) and ^{13}C chemical shifts of the solvent as secondary standards. ^{31}P NMR data is reported relative to external H_3PO_4 and ^{19}F NMR data is reported relative to external trifluorotoluene. ^{11}B NMR is reported relative to an external sample of $BF_3 \cdot OEt_2$. Infrared spectroscopy was performed using KBr pellets on a Bruker VERTEX 70 spectrophotometer with an MCT detector. Elemental analyses were performed at Robertson Microlit Laboratories Inc. (Ledgewood, NJ). Solution state magnetic susceptibility was determined via Evans method at 25 °C using the Varian 500-MR NMR spectrometer. UV-Vis measurements were conducted using a Hitachi U-2010 spectrophotometer in quartz cuvettes with a path length of 1 cm.

X-ray Crystallography: Diffraction data were collected and analyzed at Arizona State University. Single crystals suitable for X-ray diffraction were coated with polyisobutylene oil in the glovebox and transferred to a glass fiber with Apiezon N grease before mounting on the goniometer head of a Bruker APEX Diffractometer equipped with Mo Kα radiation. A hemisphere routine was used for data collection and determination of the lattice constants. The space group was identified and the data was processed using the Bruker SAINT+ program and corrected for absorption using SADABS. The structures were solved using direct methods (SHELXS) completed by subsequent Fourier synthesis and refined by full-matrix, least-squares procedures on [F^2] (SHELXL). The crystallographic parameters determined for **2**, **3-Et$_2$O**, **3-MTBE**, and **4** are provided in Table S4 and Table S7.

EPR Spectroscopy:

Instrumentation. Studies were performed at the EPR Facility of Arizona State University. Continuous wave (CW) EPR spectra were recorded at 120 and 296 K using a Bruker ELEXSYS E580 CW X-band spectrometer (Bruker, Rheinstetten, Germany). A standard resonator (ER 4102ST) attached to a liquid nitrogen temperature control system (ER 4131VT) was used at 120 K, whereas a cylindrical mode resonator (ER 4103TM) was used at 296 K. The magnetic field modulation frequency was 100 kHz with a field modulation amplitude of 0.2 mT (at 120 K) and

0.5 mT (at 296 K) peak-to-peak. The microwave power was 0.25 mW, the microwave frequency was 9.40 GHz (at 120 K) and 9.73 GHz (at 296 K), and the sweep time was 168 seconds (at 120 K) and 84 seconds (at 296 K).

Spin Hamiltonian. The EPR spectra of **2** were interpreted using a spin Hamiltonian, *H*, containing the electron Zeeman interaction with the applied magnetic field B_o and hyperfine coupling (hfc) interactions with three ^1H (I = ½), two of them being equivalent:[43]

$$H = \beta_e \boldsymbol{S}.\boldsymbol{g}.\mathbf{B_o} + \sum_{i=1}^{2} h\,\boldsymbol{S}.\boldsymbol{A}^{H_i}.\boldsymbol{I}^{H_i} + h\,\boldsymbol{S}.\boldsymbol{A}^{H_3}.\boldsymbol{I}^{H_3} \qquad (6)$$

where $\boldsymbol{S}$ is the electron spin operator, $\boldsymbol{I}^{H_i}$ and $\boldsymbol{I}^{H_3}$ are the nuclear spin operators of the two equivalent protons and the single one, respectively, $\boldsymbol{A}^{H_i}$ and $\boldsymbol{A}^{H_3}$ are the corresponding hfc tensors in frequency units, $\boldsymbol{g}$ is the electronic *g*-tensor, β_e is the electron magneton, and *h* is Planck's constant.

Fitting of EPR spectra. To quantitatively compare experimental and simulated spectra, we divided the spectra into N intervals, i.e. we treated the spectrum as an N-dimensional vector **R**. Each component R_j has the amplitude of the EPR signal at a magnetic field B_j, with j varying from 1 to N. The amplitudes of the experimental and simulated spectra were normalized so that the span between the maximum and minimum values of R_j is 1. We compared the calculated amplitudes R_j^{calc} of the signal with the observed values R_j defining a root-mean-square deviation σ by:

$$\sigma(p_1, p_2, \ldots, p_n) = [\sum_j (R_j^{calc}(p_1, p_2, \ldots, p_n) - R_j^{exp})^2/N]^{1/2} \qquad (7)$$

where the sums are over the N values of j, and p's are the fitting parameters that produced the calculated spectrum. For our simulations, N was set equal to 1024. The EPR spectra were simulated using EasySpin (v 5.2.11), a computational package developed by Stoll and Schweiger[44] and based on Matlab (The MathWorks, Natick, MA, USA). EasySpin calculates EPR resonance fields using the energies of the states of the spin system obtained by direct diagonalization of the spin Hamiltonian (see Eq. 6). The EPR fitting procedure used a Monte Carlo type iteration to minimize the root-mean-square deviation, σ (see Eq. 7) between measured and simulated spectra. We searched for the optimum values of the following parameters: the principal components of $\boldsymbol{g}$ (i.e. g_x, g_y, g_z), the principal components of the hfc tensors $\boldsymbol{A}^{H_i}$ (i.e. $A_x^{H_i}$, $A_y^{H_i}$, $A_z^{H_i}$) and $\boldsymbol{A}^{H_3}$ (i.e. $A_x^{H_3}$, $A_y^{H_3}$, $A_z^{H_3}$) and the peak-to-peak line-widths (ΔB_x, ΔB_y, ΔB_z).

Cyclic Voltammetry: All experiments were carried out under N_2 atmosphere using a CH Instruments 1200 potentiostat with a three-electrode system consisting of a 3 mm diameter glassy carbon working electrode, a silver wire pseudo reference electrode, and a platinum counter electrode. The working electrode was cleaned by successive polishing with 1.0 and 0.3 μm Alumina slurries followed by thorough washing with ultrapure water. The Ag wire was dipped into 1 M HCl and air-dried prior to use. The electrolyte solution used was 0.1 M $TBAPF_6$ in acetonitrile. All potentials are reported relative to ferrocene, which was used as internal standard.

Computational Details: Calculations were performed using the Gaussian 09 suite.[45] Geometry optimization was carried out using PBE[46] with 6-31g(d, p) basis set.[47] Single point energy calculations were conducted using PBE and either 6-311g(d, p) or 6-311++g(2d, p) basis sets.[48] A single point energy calculation was also performed on the crystal structure geometry of **2** using B3LYP[49-53] and similar orbital population was obtained. The molecular orbitals were visualized in Chemissian[54] (version 4.53) using the results of the PBE/6-311++g(2d, p) calculation. The optimized Cartesian coordinates are listed in Table S10 and the bond distances and angles are shown in Table S2. The energies obtained from the different calculation methods are tabulated in Table S3.

Synthesis of (^{Ph2PPr}PDI)Mn(CO) (2): A 20 mL scintillation vial was charged with **[**(^{Ph2PPr}PDI)Mn(CO)][Br] (**1**) (0.109 g, 0.1403 mmol) and 10 mL THF was added. To the slurry, freshly cut metallic Na (0.0162 g, 0.702 mmol) was added and stirred for 6 h at ambient temperature. The resulting dark purple solution was filtered through Celite and THF was removed under vacuum. The solid was dissolved in 10 mL of toluene and filtered through Celite to remove any remaining NaBr salt. After toluene removal and washing with diethyl ether (2 x 5 mL), the residue was dried thoroughly to isolate a purple solid identified as (^{Ph2PPr}PDI)Mn(CO) (**2**) (0.043 g, 0.0616 mmol, 44% yield). X-ray quality crystals were obtained by cooling a concentrated toluene solution layered with diethyl ether for 12 h. Elemental analysis for $C_{40}H_{41}N_3MnP_2O$: Calcd. C, 68.96; H, 5.93, N, 6.03. Found: C, 68.39, 6.38, 5.71. Magnetic susceptibility (Evans method, 25 °C) μ_{eff} = 1.97 μ_B. ^{1}H NMR (benzene-d_6, 25 °C): δ 10.64 (50% linewidth = 423.48 Hz), 9.32 (50% linewidth = 369.87 Hz), 8.97 (50% linewidth = 150.70 Hz), 5.52 (50% linewidth = 97.69 Hz). No ^{13}C and ^{31}P NMR resonances observed. IR (neat, KBr): ν (cm^{-1}) 3053, 3047, 2923, 2898, 2869, 2852, 1782 (CO), 1583, 1569, 1479, 1431, 1406, 1327,

1255, 1213, 1157, 1091, 1041. UV/Vis (toluene, 25 °C, absorption coefficients determined by plotting absorptions against multiple concentrations using the Beer-Lambert equation): 335 nm (17600 $M^{-1}cm^{-1}$), 395 nm (14000 $M^{-1}cm^{-1}$), 538 nm (14400 $M^{-1}cm^{-1}$), 674 nm (4000 $M^{-1}cm^{-1}$).

Synthesis of [(κ^4-^{Ph2PPr}PDI)Mn(μ-η^1,η^1,η^2-CO)K(Et_2O)]$_2$ (3-Et_2O): A 20 mL scintillation vial was charged with Hg (2.36 g, 11.85 mmol) and approximately 5 mL of dry THF was added to it. Freshly cut K metal (0.0136 g, 0.592 mmol) was then added to the vial and vigorously stirred for 30 min. To the resulting amalgam, a 10 mL THF slurry of **1** (0.092 g, 0.119 mmol) was added and stirred at ambient temperature for 7 h. The dark brown solution was then vacuum filtered through Celite and THF was removed *in vacuo*. To the resulting solid, 5 mL of Et_2O was added, layered with 1 mL of pentane, and placed at -35 °C. Green crystals were obtained after 24 h, which were identified as [(κ^4-^{Ph2PPr}PDI)Mn(μ-η^1,η^1,η^2-CO)K(Et_2O)]$_2$ (**3-Et_2O**) (0.043 g, 45%). Elemental analysis for $C_{88}H_{102}N_6Mn_2P_4O_4K_2$: Calcd. C, 65.25; H, 6.35; N, 5.19. Found: C, 64.50; H, 6.16; N, 5.14. ^{1}H NMR (benzene-d_6, 25 °C): δ 8.05 (d, J = 7.2 Hz, 1H, *m-pyridine*), 7.94 (d, J = 7.0 Hz, 1H, *m-pyridine*), 7.61 (m, 3H, *phenyl*), 7.37 (m, 4H, *phenyl*), 7.21 (m, 2H, *phenyl*), 7.14 – 7.07 (m, 2H, *phenyl*), 7.07 – 7.02 (m, 3H, *phenyl*), 6.99 (m, 2H, *phenyl*), 6.54 (m, 1H, *phenyl*), 6.51 (m, 2H, *phenyl*), 5.46 (t, J = 7.4 Hz, 2H, *phenyl*), 5.06 (d, J = 8.7 Hz, 1H, CH_2), 4.64 (m, 1H, CH_2), 4.46 (m, 1H, CH_2), 3.95 (m, 1H, CH_2), 3.25 (q, J = 7.0 Hz, 4H, CH_2-coordinated Et_2O), 2.98 (t, J = 12.2 Hz, 1H, CH_2), 2.80 (s, 3H, PDI-CH_3), 2.65 (s, 3H, PDI-CH_3), 2.55 (t, J = 12.4 Hz, 1H, CH_2), 2.32 (dd, J = 35.1, 13.2 Hz, 1H, CH_2), 1.91 (m, 4H, CH_2), 1.37 (m, 1H, CH_2), 1.10 (t, J = 7.0 Hz, 6H, CH_3-coordinated Et_2O).^{13}C NMR (benzene-d_6, 25 °C): δ 245.95 (*C*O), 144.56 (*phenyl*), 144.33 (*phenyl*), 139.92 (*phenyl*), 139.82 (*phenyl*), 139.04 (*phenyl*), 136.59 (*phenyl*), 136.17 (*phenyl*), 135.85 (*phenyl*), 133.51 (*phenyl*), 133.14 (*phenyl*), 131.49 (*phenyl*), 129.30 (*phenyl*), 129.14 (*phenyl*), 129.09 (*phenyl*), 128.83 (*phenyl*), 127.87 (*phenyl*), 113.11 (*p-pyridine*), 106.63 (*m-pyridine*), 106.17 (*m-pyridine*), 66.23 (*C*H_2-coordinated Et_2O), 63.53 (*C*H_2), 59.31 (*C*H_2), 34.78 (imine-*C*), 33.39 (*C*H_2), 30.54 (*C*H_2), 29.99 (*C*H_2), 26.22 (*C*H_2), 15.92 (*C*H_3-coordinated Et_2O), 14.42 (PDI-*C*H_3). ^{31}P NMR (benzene-d_6, 25 °C): δ (ppm) 82.07 (s, Ph_2P), -16.37 (s, Ph_2P). IR (neat, KBr): ν (cm^{-1}) 3047, 2960, 2927, 2852, 1816, 1710 (CO), 1656 (CO), 1550, 1432, 1381, 1321, 1171, 1095. UV/Vis (toluene, 25 °C, absorption coefficients determined by plotting absorptions against multiple concentrations using the Beer-Lambert equation): 339 nm (30500 $M^{-1}cm^{-1}$), 447 nm (20300 $M^{-1}cm^{-1}$).

Synthesis of [(κ^4-^{Ph2PPr}PDI)Mn(μ-η^1,η^1-CO)K(^{t}BuOMe)$_2$]$_2$ (3-MTBE): A 20 mL scintillation vial was charged with Hg (3.12 g, 15.60 mmol) and approximately 5 mL of dry THF was added to it. Freshly cut K metal (0.0304 g, 0.779 mmol) was then added to the Hg and vigorously stirred for 30 min. To the resulting amalgam, a 10 mL THF slurry of **1** (0.121g, 0.156 mmol) was added and stirred at ambient temperature for 14 h. The dark green solution was then vacuum filtered through Celite and THF was removed *in vacuo*. The resulting solid was dissolved in 10 mL of toluene and filtered through Celite. Toluene was evacuated and the residue was dissolved in 2-3 mL of ^{t}BuOMe and the resulting dark green solution was placed at -35 °C after layering with pentane. Removal of the supernatant and drying thoroughly yielded greenish crystalline solid identified as [(κ^4-^{Ph2PPr}PDI)Mn(μ-η^1,η^1-CO)K(^{t}BuOMe)$_2$]$_2$ (**3-MTBE**) (0.095 g, 33%). X-ray diffraction analysis of the crystals before drying showed two MTBE molecules coordinated to each K^+ ion. Elemental analysis for $C_{90}H_{106}N_6Mn_2P_4O_4K_2$: Calcd. C, 65.60; H, 6.48; N, 5.10. Found: C, 64.32; H, 6.08; N, 5.11. ^{1}H NMR (benzene-d_6, 25 °C) δ 8.06 (d, J = 7.4 Hz, 1H, *m*-pyridine), 7.94 (d, J = 7.5 Hz, 1H, *m*-pyridine), 7.60 (m, 3H, *phenyl* and *p-pyridine*), 7.35 (q, J = 6.9 Hz, 4H, *phenyl*), 7.20 (t, J = 7.3 Hz, 2H, *phenyl*), 7.11-7.08 (m, 3H, *phenyl*), 7.05 – 7.00 (m, 2H, *phenyl*), 7.00 – 6.94 (m, 2H, *phenyl*), 6.59-6.53 (m, 1H, *phenyl*), 6.51 (t, J = 7.0 Hz, 2H, *phenyl*), 5.46 (t, J = 8.0 Hz, 2H, NCH_2), 5.07 (d, J = 8.8 Hz, 1H, CH_2), 4.67 (t, J = 11.8 Hz, 1H, CH_2), 4.46 (m, 1H, CH_2), 3.94 (m, 1H, CH_2), 3.03 (s, 3H, ^{t}BuO*Me*), 2.98 (d, J = 13.6 Hz, 1H), 2.80 (s, 3H, PDI-CH_3), 2.64 (s, 3H, PDI-CH_3), 2.55 (t, J = 12.6 Hz, 1H, CH_2), 2.32 (dd, J = 35.3, 14.1 Hz, 1H, CH_2), 2.06 – 1.75 (m, 4H, CH_2), 1.44 – 1.29 (m, 2H, CH_2), 1.07 (s, 9H, ^{t}*Bu*OMe). ^{13}C NMR (benzene-d_6, 25 °C): δ 245.85 (CO), 144.53 (*phenyl*), 144.31 (*phenyl*), 140.87 (*phenyl*), 139.99 (*phenyl*), 139.82 (*phenyl*), 139.16 (*phenyl*), 139.04 (*phenyl*), 136.64 (*phenyl*), 136.10 (*phenyl*), 135.78 (*phenyl*), 133.50 (*phenyl*), 133.29 (*phenyl*), 133.14 (*phenyl*), 133.03 (*phenyl*), 131.48 (*phenyl*), 129.30 (*phenyl*), 129.15 (*phenyl*), 128.82 (*phenyl*), 127.87 (*phenyl*), 113.13 (*p-pyridine*), 106.66 (*m-pyridine*), 106.20 (*m-pyridine*), 72.59 (*C*Me$_3$), 63.58 (*C*H$_2$), 59.35 (*C*H$_2$), 49.49 (^{t}BuO*C*H$_3$), 33.57 (*C*H$_2$), 30.55 (*C*H$_2$), 29.96 (*C*H$_2$), 27.39 (C*Me$_3$*), 26.22 (*C*H$_2$), 14.63 (*C*H$_3$-PDI), 14.46 (*C*H$_3$-PDI). ^{31}P NMR (benzene-d_6, 25 °C): δ (ppm) 82.79 (s, Ph$_2$*P*), -15.69 (s, Ph$_2$*P*). IR (neat, KBr): ν (cm^{-1}) 3047, 2970, 2929, 2900, 2870, 1813, 1695 (CO), 1579, 1549, 1431, 1362, 1321, 1196, 1176, 1070, 1018. UV/Vis (toluene, 25 °C, absorption coefficients determined by plotting absorptions against multiple concentrations using the Beer-Lambert equation): 338 nm (57600 M^{-1}cm^{-1}), 440 nm (39100 M^{-1}cm^{-1}).

Synthesis of (κ^4-^{Ph2PPr}PDI)Mn(μ-η^1,η^2-CO)K(18-crown-6) (4): *Method A.* A 20 mL scintillation vial was charged with Hg (4.76 g, 23.82 mmol) and approximately 5 mL of dry THF was added to it. Freshly cut K metal (0.0465 g, 1.191 mmol) was then added to the Hg and vigorously stirred for 30 min. To the resulting amalgam, a 10 mL THF slurry of **1** (0.185 g, 0.238 mmol) was added followed by 18-crown-6 (0.079 g, 0.298 mmol). The mixture was stirred at ambient temperature for 12 h. The dark greenish-brown solution was then vacuum filtered through Celite and THF was removed *in vacuo*. The resulting solid was dissolved in 10 mL of toluene and filtered through Celite. Removal of toluene followed by washing with Et_2O and drying afforded a dark brownish-green powder identified as (κ^4-^{Ph2PPr}PDI)Mn(μ-η^1,η^2-CO)K(18-crown-6) (**4**) (0.190 g, 79% yield). X-ray quality crystals were obtained by cooling a concentrated diethyl ether solution at -35 °C for 15 h. *Method B.* To a benzene-d_6 solution of **3-Et$_2$O** (0.015 g, 0.0093 mmol) or **3-MTBE** (0.0148 g, 0.0089 mmol) separately, was added 18-crown-6 (0.00489 g, 0.0185 mmol or 0.00475 g, 0.0179 mmol, respectively). An instant color change from deep green to brown was noticed in both cases. Complete conversion to **4** was observed by ^{1}H and ^{31}P NMR spectroscopy. Benzene-d_6 was removed *in vacuo,* the residue was washed with pentane (2 x 4 mL), and dried thoroughly under vacuum to isolate brownish-green powder (89% and 92% yields, respectively). Elemental analysis for $C_{52}H_{65}N_3MnP_2O_7K$: Calcd. C, 62.45; H, 6.55; N, 4.20. Found: C, 62.21; H, 6.77; N, 4.13. ^{1}H NMR (benzene-d_6, 25 °C) δ 8.02 (d, *J* = 7.5 Hz, 1H, *m-pyridine*), 7.91 (t, *J* = 7.9 Hz, 2H, *phenyl*), 7.80 (d, *J* = 7.5 Hz, 1H, *m-pyridine*), 7.60 (t, *J* = 6.9 Hz, 2H, *phenyl*), 7.53 – 7.48 (m, 2H, *phenyl*), 7.45 (t, *J* = 7.6 Hz, 1H, *p-pyridine*), 7.28 (t, *J* = 7.7 Hz, 2H, *phenyl*), 7.22 (t, *J* = 7.2 Hz, 2H, *phenyl*), 7.14 – 7.03 (m, 5H, *phenyl*), 6.60 (d, *J* = 5.0 Hz, 3H, *phenyl*), 5.62 – 5.55 (m, 2H, *phenyl*), 5.16 (d, *J* = 8.9 Hz, 2H, C*H*$_2$), 4.57 (td, *J* = 11.9, 4.4 Hz, 1H, C*H*$_2$), 4.26 (td, *J* = 12.0, 4.9 Hz, 1H, C*H*$_2$), 3.52 (m, 1H, C*H*$_2$P), 2.94 (s, 3H, C*H*$_3$), 2.90 (s, 24H, 18-crown-6 C*H*$_2$), 2.70 (s, 3H, C*H*$_3$), 2.62 – 2.50 (m, 1H, C*H*$_2$), 2.38 (m, 1H, C*H*$_2$), 2.32 – 2.22 (m, 1H, C*H*$_2$), 2.07 – 1.97 (m, 1H, C*H*$_2$), 1.97 – 1.83 (m, 1H, C*H*$_2$), 1.56 (s, 1H, C*H*$_2$), 1.25 (m, 1H, C*H*$_2$). ^{13}C NMR (benzene-d_6, 25 °C): δ (ppm) 245.31 (CO), 145.36 (*phenyl*), 145.10 (*phenyl*), 140.89 (*phenyl*), 139.11 (*phenyl*), 136.53 (*phenyl*), 134.76 (*phenyl*), 133.92 (*phenyl*), 133.73 (*phenyl*), 133.66 (*phenyl*), 133.52 (*phenyl*), 133.28 (*phenyl*), 133.11 (*phenyl*), 131.75 (*phenyl*), 129.06 (*phenyl*), 128.99 (*phenyl*), 127.77 (*phenyl*), 127.68 (*phenyl*), 128.27 (*phenyl*), 111.98 (*p-pyridine*), 104.28 (*m-pyridine*), 103.76 (*m-pyridine*), 70.08 (18-crown-6 *C*H$_2$), 64.06 (*C*H$_2$), 59.16 (*C*H$_2$), 33.12 (*C*H$_2$), 29.54 (*C*H$_2$), 27.04 (*C*H$_2$),

22.97 (*C*H_2), 14.84 (*C*H_3), 14.50 (*C*H_3). ^{31}P NMR (benzene-d_6, 25 °C): δ (ppm) 86.27 (s, coordinated Ph_2P), -15.69 (s, uncoordinated Ph_2P). IR (neat, KBr): ν (cm^{-1}) 3048, 2887, 2861, 1821, 1697 (CO), 1583, 1554, 1471, 1452, 1433, 1351, 1326, 1251, 1111, 1070, 1025. UV/Vis (toluene, 25 °C, absorption coefficients determined by plotting absorptions against multiple concentrations using the Beer-Lambert equation): 346 nm (14700 $M^{-1}cm^{-1}$), 415 nm (11800 $M^{-1}cm^{-1}$), 512 nm (7000 $M^{-1}cm^{-1}$), 621 nm (2900 $M^{-1}cm^{-1}$).

Observation of [(^{Ph2PPr}PDI)Mn(CO)][OTf] (5): A 20 mL scintillation vial was charged with **4** (0.067 g, 0.0669 mmol) in approximately 6 mL THF. Two equivalents of trifluoromethanesulfonic acid (12 μL, 0.134 mmol) were added to the greenish-brown solution, which turned immediately into a bright purple solution. The solution was swirled for two minutes and upon cooling at -35 °C overnight, a colorless side product (presumed to be [CF_3SO_3][K(18-crown-6)]) crystallized (a small quantity of this side product remained with **5** and was found to be inseparable because of similar solubility). The supernatant was filtered through Celite, concentrated to dryness, washed with diethyl ether (4 x 3 mL) and finally dried thoroughly to isolate a purple solid (0.048 g, 78%) identified as [(^{Ph2PPr}PDI)Mn(CO)][OTf] (**5**). ^{1}H NMR (acetonitrile-d_3, 25 °C): δ. 7.45 (m, br, 4H, *phenyl*), 7.36 (m, br, 6H, *phenyl*), 7.22 (m, br, 1H, *p-pyridine*), 7.11 (m, br, 2H, *m-pyridine*), 6.95 (m, br, 2H, *phenyl*), 6.91 (m, br, 4H, *phenyl*), 6.44 (m, br, 4H, *phenyl*), 4.39 (m, br, 2H, CH_2), 3.87 (m, br, 2H, CH_2), 2.67 (m, br, 2H, CH_2), 2.55 (m, br, 2H, CH_2), 2.44 (m, br, 2H, CH_2), 2.24 (s, br, 6H, CH_3), 2.13 (m, br, 2H, CH_2). ^{13}C NMR (acetonitrile-d_3, 25 °C): δ 166.94 (*C-pyridine*), 165.17 (*phenyl*), 157.34 (*phenyl*), 137.25 (m, *C*F_3SO_3), 132.75 (*phenyl*), 132.49 (*phenyl*), 131.59 (*phenyl*), 131.22 (*phenyl*), 130.23 (*phenyl*), 129.64 (*phenyl*), 129.23 (*phenyl*), 118.38 (*pyridine*), 58.83 (*C*H_2), 28.50 (*C*H_2), 24.80 (*C*H_2), 15.13 (*C*H_3). ^{31}P NMR (acetone-d_6, 25 °C): δ 53.79 (s, Ph_2P). ^{19}F NMR (acetonitrile-d_3, 25 °C): δ −79.30 (OTf). IR (KBr neat): ν (cm^{-1}) 3055, 2916, 2891, 1954, 1909, 1834 (CO), 1666, 1581, 1483, 1435, 1354, 1275, 1225, 1161, 1109, 1030. UV/Vis (acetonitrile, 25 °C, absorption coefficients determined by plotting absorptions against multiple concentrations using the Beer-Lambert equation): 311 nm (4600 $M^{-1}cm^{-1}$), 370 nm (2200 $M^{-1}cm^{-1}$), 527 nm (3800 $M^{-1}cm^{-1}$), 677 nm (440 $M^{-1}cm^{-1}$).

Observation of [(^{Ph2PPr}PDI)Mn(CO)][BF_4] (6): A 20 mL scintillation vial was charged with **4** (0.051 g, 0.05099 mmol) in approximately 6 mL THF. Two equivalents of $HBF_4 \cdot OEt_2$ (14.7 μL, 0.1071 mmol) were added to the greenish-brown solution, which turned immediately into a

bright purple solution. The solution was swirled for two minutes and upon cooling at -35 °C overnight, a colorless side product (presumed to be $[BF_4][K(18\text{-crown-6})]$) crystallized (a small quantity of this side product remained with **6** and was found to be inseparable because of similar solubility). The supernatant was filtered through Celite, concentrated to dryness, washed with diethyl ether (4 x 3 mL), and dried thoroughly to isolate a purple solid (0.024 g, 62%) identified as $[(^{Ph2PPr}PDI)Mn(CO)][BF_4]$ (**6**). ^{1}H NMR (acetonitrile-d_3, 25 °C): δ 7.43 (m, 4H, *phenyl*), 7.34 (m, 4H, *phenyl*), 7.20 (t, J = 7.0 Hz, 1H, *p-pyridine*), 7.09 (t, J = 6.9 Hz, 2H, *phenyl*), 6.94 (d, J = 7.6 Hz, 2H, *m-pyridine*), 6.89 (m, 4H, *phenyl*), 6.42 (m, 4H, *phenyl*), 4.37 (d, J = 10.4 Hz, 1H, CH_2), 3.86 (m, 6H, CH_2), 2.65 (t, J = 13.1 Hz, 2H, CH_2), 2.53 (t, J = 14.7 Hz, 2H, CH_2), 2.44 (m, 1H, CH_2), 2.22 (s, 6H). ^{13}C NMR (acetonitrile-d_3, 25 °C): δ 165.17 (*phenyl*), 157.40 (*phenyl*), 132.80 (*p-pyridine*), 132.52 (*phenyl*), 131.63 (*phenyl*), 131.27 (*phenyl*), 130.27 (*phenyl*), 129.69 (*phenyl*), 129.27 (*phenyl*), 118.42 (*m-pyridine*), 58.88 (CH_2), 28.54 (CH_3), 24.61 (CH_2), 15.14 (CH_2). ^{31}P NMR (acetonitrile-d_3, 25 °C): δ 55.84 (s, Ph_2P). ^{19}F NMR (acetonitrile-d_3, 25 °C): δ –151.78 ppm (broad). ^{11}B NMR (acetonitrile-d_3, 25 °C): δ –2.45 ppm (BF_4). IR (KBr neat): ν (cm^{-1}) 3265, 3201, 2912, 2827, 1952, 1909, 1835, 1699, 1649, 1583, 1458, 1435, 1354, 1286, 1250. UV/Vis (acetonitrile, 25 °C, absorption coefficients determined by plotting absorptions against multiple concentrations using the Beer-Lambert equation): 315 nm (3000 $M^{-1}cm^{-1}$), 370 nm (1500 $M^{-1}cm^{-1}$), 526 nm (2500 $M^{-1}cm^{-1}$), 677 nm (300 $M^{-1}cm^{-1}$).

ASSOCIATED CONTENT

Supporting Information

The Supporting Information is available free of charge on the ACS Publications website. Compound characterization, cyclic voltammograms, and metrical parameters for **2, 3-Et$_2$O, 3-MTBE**, and **4**.

Accession Codes

CCDC 1821719 and **1821720** contains the supplementary crystallographic data for this paper. These data can be obtained free of charge via www.ccdc.cam.ac.uk/data_request/cif, by emailing data_request@ccdc.cam.ac.uk, or by contacting The Cambridge Crystallographic Data Centre, 12 Union Road, Cambridge CB2 1EZ, UK; fax: +441223336033.

AUTHOR INFORMATION

Corresponding Author

*(R. J. T.) Phone: 480-727-8930. Email: ryan.trovitch@asu.edu

Author Contributions

The manuscript was written through contributions of all authors. All authors have given approval to the final version of the manuscript.

Notes

The authors declare no competing financial interest.

ACKNOWLEDGMENT

This material is based upon work supported by the National Science Foundation under Grant No. 1651686. R. J. T. and T. K. M would also like to thank the Donors of the American Chemical Society Petroleum Research Fund and the Research Corporation for Science Advancement for support.

ABBREVIATIONS

PDI: 2,6-bis(imino)pyridine (or pyridine diimine); NMR: nuclear magnetic resonance; EPR: electron paramagnetic resonance; DFT: density functional theory; SOMO: singly-occupied molecular orbital; THF: tetrahydrofuran; MTBE: methyl *tert*-butyl ether; OTf: triflate.

REFERENCES

1. Berardi, S.; Drouet, S.; Francas, L.; Gimbert-Surinach, C.; Guttentag, M.; Richmond, C.; Stoll, T.; Llobet, A. "Molecular artificial photosynthesis." *Chem. Soc. Rev.* **2014**, *43*, 7501−7519.
2. Keith, J. A.; Grice, K. A.; Kubiak, C. P.; Carter, E. A. "Elucidation of the Selectivity of Proton-Dependent Electrocatalytic CO_2 Reduction by *fac*-Re(bpy)$(CO)_3$Cl." *J. Am. Chem. Soc.* **2013**, *135*, 15823-15829.
3. Windle, C. D.; Perutz, R. N. "Advances in molecular photocatalytic and electrocatalytic CO_2 reduction." *Coord. Chem. Rev.* **2012**, *256*, 2562-2570.
4. Benson, E. E.; Kubiak, C. P.; Sathrum, A. J.; Smieja, J. M. "Electrocatalytic and homogeneous approaches to conversion of CO_2 to liquid fuels." *Chem. Soc. Rev.* **2009**, *38*, 89-99.

5. Dubois, M. R.; Dubois, D. L. "Development of Molecular Electrocatalysts for CO_2 Reduction and H_2 Production/Oxidation." *Acc. Chem. Res.* **2009**, *42*, 1974-1982.
6. Ngo, K. T.; McKinnon, M.; Mahanti, B.; Narayanan, R.; Grills, D. C.; Ertem, M. Z.; Rochford, J. "Turning on the Protonation-First Pathway for Electrocatalytic CO_2 Reduction by Manganese Bipyridyl Tricarbonyl Complexes." *J. Am. Chem. Soc.* **2017**, *139*, 2604-2618.
7. Sampson, M. D.; Kubiak, C. P. "Manganese Electrocatalysts with Bulky Bipyridine Ligands: Utilizing Lewis Acids To Promote Carbon Dioxide Reduction at Low Overpotentials." *J. Am. Chem. Soc.* **2016**, *138*, 1386-1393.
8. Vollmer, M. V.; Machan, C. W.; Clark, M. L.; Antholine, W. E.; Agarwal, J.; Schaefer, H. F.; Kubiak, C. P.; Walensky, J. R. "Synthesis, Spectroscopy, and Electrochemistry of (α-Diimine)$M(CO)_3Br$, M=Mn, Re, Complexes: Ligands Isoelectronic to Bipyridyl Show Differences in CO_2 Reduction." *Organometallics* **2015**, *34*, 3-12.
9. Riplinger, C.; Carter, E. A. "Influence of Weak Brønsted Acids on Electrocatalytic CO_2 Reduction by Manganese and Rhenium Bipyridine Catalysts." *ACS Catalysis* **2015**, *5*, 900-908.
10. Sampson, M. D.; Nguyen, A. D.; Grice, K. A.; Moore, C. E.; Rheingold, A. L.; Kubiak, C. P. "Manganese Catalysts with Bulky Bipyridine Ligands for the Electrocatalytic Reduction of Carbon Dioxide: Eliminating Dimerization and Altering Catalysis." *J. Am. Chem. Soc.* **2014**, *136*, 5460-5471.
11. Zeng, Q.; Tory, J.; Hartl, F. "Electrocatalytic Reduction of Carbon Dioxide with a Manganese(I) Tricarbonyl Complex Containing a Nonaromatic α-Diimine Ligand." *Organometallics* **2014**, *33*, 5002-5008.
12. Sampson, M. D.; Froehlich, J. D.; Smieja, J. M.; Benson, E. E.; Sharp, I. D.; Kubiak, C. P. "Direct observation of the reduction of carbon dioxide by rhenium bipyridine catalysts." *Energ. Environ. Sci.* **2013**, *6*, 3748-3755.
13. Grice, K. A.; Gu, N. X.; Sampson, M. D.; Kubiak, C. P. "Carbon monoxide release catalysed by electron transfer: electrochemical and spectroscopic investigations of [Re(bpy-R)$(CO)_4$](OTf) complexes relevant to CO_2 reduction." *Dalton Trans.* **2013**, *42*, 8498-8503.
14. Smieja, J. M.; Sampson, M. D.; Grice, K. A.; Benson, E. E.; Froehlich, J. D.; Kubiak, C. P. "Manganese as a Substitute for Rhenium in CO_2 Reduction Catalysts: The Importance of Acids." *Inorg. Chem.* **2013**, *52*, 2484-2491.

15. Bourrez, M.; Molton, F.; Chardon-Noblat, S.; Deronzier, A. "[Mn(bipyridyl)$(CO)_3$Br]: An Abundant Metal Carbonyl Complex as Efficient Electrocatalyst for CO_2 Reduction." *Angew. Chem., Int. Ed*. **2011**, *50*, 9903−9906.
16. Smieja, J. M.; Kubiak, C. P. "Re(bipy-tBu)$(CO)_3$Cl-improved Activity for Reduction of Carbon Dioxide: IR-Spectroelectrochemical and Mechanistic Studies." *Inorg. Chem*. **2010**, *49*, 9283−9289.
17. Kumar, B.; Smieja, J. M.; Kubiak, C. P. "Photoreduction of CO_2 on p-type Silicon Using Re(bipy-Bu^t)$(CO)_3$Cl: Photovoltages Exceeding 600 mV for the Selective Reduction of CO_2 to CO." *J. Phys. Chem. C* **2010**, *114*, 14220−14223.
18. Johnson, F. P. A.; George, M. W.; Hartl, F.; Turner, J. J. "Electrocatalytic Reduction of CO_2 Using the Complexes $[Re(bpy)(CO)_3L]^n$ (n = +1, L = $P(OEt)_3$, CH_3CN; n = 0, L = Cl^-, Otf^-; bpy = 2,2'-Bipyridine; Otf^- = CF_3SO_3) as Catalyst Precursors: Infrared Spectroelectrochemical Investigation." *Organometallics* **1996**, *15*, 3374−3387.
19. Sullivan, B. P.; Bolinger, C. M.; Conrad, D.; Vining, W. J.; Meyer, T. J. "One- and two-electron pathways in the electrocatalytic reduction of CO_2 by *fac*-Re(bpy)$(CO)_3$Cl (bpy = 2,2'-bipyridine." *J. Chem. Soc., Chem. Commun.* **1985**, 1414−1416.
20. Hawecker, J.; Lehn, J.-M.; Ziessel, R. "Electrocatalytic reduction of carbon dioxide mediated by Re(bipy)$(CO)_3$Cl (bipy = 2,2'-bipyridine)." *J. Chem. Soc., Chem. Commun*. **1984**, 328−330.
21. Valyaev, D. A.; Lavigne, G.; Lugan, N. "Manganese organometallic compounds in homogeneous catalysis: Past, present, and prospects." *Coord. Chem. Rev.* **2016**, *308*, 191-235.
22. Valyaev, D. A.; Peterleitner, M. G.; Semeikin, O. V.; Utegenov, K. I.; Ustynyuk, N. A.; Sournia-Saquet, A.; Lugan, N; Lavigne, G. "Proton reduction catalysis by manganese vinylidene and allenylidene complexes." *J. Organomet. Chem.* **2007**, *692*, 3207-3211.
23. Hou, K.; Poh, H. T.; Fan, W. Y. "Electrocatalytic hydrogen generation by a trithiolato-bridged dimanganese hexacarbonyl anion with a turnover frequency exceeding 40000 s^{-1}." *Chem. Commun.* **2014**, *50*, 6630-6632.
24. Hou, K.; Fan, W. Y. "Electrocatalytic proton reduction catalyzed by a dimanganese disulfide carbonyl complex containing a redox-active internal disulfide bond." *Dalton Trans.* **2014**, *43*, 16977-16980.

25. Hou, K.; Lauw, S. J. L.; Webster, R. D.; Fan, W. Y. "Electrochemical proton reduction catalysed by selenolato-manganese carbonyl complexes." *RSC Adv.* **2015**, *5*, 39303-39309.
26. Sampson, M. D.; Kubiak, C. P. "Electrocatalytic Dihydrogen Production by an Earth-Abundant Manganese Bipyridine Catalyst." *Inorg. Chem.* **2015**, *54*, 6674-6676.
27. Mukhopadhyay, T. K.; MacLean, N. L.; Gan, L.; Ashley, D. C.; Groy, T. L.; Baik, M.-H.; Jones, A. K.; Trovitch, R. J. "Carbon Dioxide Promoted H^+ Reduction Using a Bis(imino)pyridine Manganese Electrocatalyst." *Inorg. Chem.* **2015**, *54*, 4475-4482.
28. Appel, A. M.; Helm, M. L. "Determining the Overpotential for a Molecular Electrocatalyst." *ACS Catal.* **2014**, *4*, 630-633.
29. Benson, E. E.; Sampson, M. D.; Grice, K. A.; Smieja, J. M.; Froehlich, J. D.; Friebel, D.; Keith, J. A.; Carter, E. A.; Nilsson, A.; Kubiak, C. P. "The Electronic States of Rhenium Bipyridyl Electrocatalysts for CO2 Reduction as Revealed by X-ray Absorption Spectroscopy and Computational Quantum Chemistry." *Angew. Chem. Int. Ed.* **2013**, *52*, 4841-4844.
30. Hartl, F.; Rosa, P.; Ricard, L.; Le Floch, P.; Zális, S. "Electronic transitions and bonding properties in a series of five-coordinate "16-electron" complexes $[Mn(CO)_3(L_2)]^-$ (L_2 = chelating redox-active π-donor ligand)."
31. Scarborough, C. C.; Wieghardt, K. "Electronic Structure of 2,2'-Bipyridine Organotransition-Metal Complexes. Establishing the Ligand Oxidation Level by Density Functional Theoretical Calculations." *Inorg. Chem.* **2011**, *50*, 9773-9793.
32. Knijnenburg, Q.; Gambarotta, S.; Budzelaar, P. H. M. "Ligand-centred reactivity in diiminepyridine complexes." *Dalton Trans.* **2006**, 5442−5448.
33. Bart, S. C.; Chłopek, K.; Bill, E.; Bouwkamp, M. W.; Lobkovsky, E.; Neese, F.; Wieghardt, K.; Chirik, P. J. "Electronic Structure of Bis(imino)pyridine Iron Dichloride, Monochloride, and Neutral Ligand Complexes: A Combined Structural, Spectroscopic, and Computational Study." *J. Am. Chem. Soc.* **2006**, *128*, 13901-13912.
34. Stor, G. J.; van der Vis, M.; Stufkens, D. J.; Oskam, A.; Fraanje, J.; Goubitz, K. "Coordination of the potentially tridentate ligands 2,6-diacetylpyridine-bis(anil) (dapa) and 2-(2-(2'-methylidenepyridyl)aminoethyl)pyridine (map) in the complexes *fac*-$BrMn(CO)_2L$, *fac*-$(CO)_5MM'(CO)_3L$ (M, M' = Mn, Re; L = dapa, map) and their photoproducts. The crystal structure of $BrMn(CO)_2$(N,N,N-dpa)." *J. Organomet. Chem.* **1994**, *482*, 15-29.

35. Ben-Daat, H.; Hall, G. B.; Groy, T. L.; Trovitch, R. J. "Rational Design of Rhodium Complexes Featuring κ^4-*N*,*N*,*N*,*N*- and κ^5-*N*,*N*,*N*,*P*,*P*-Bis(imino)pyridine Ligands." *Eur. J. Inorg. Chem.* **2013**, 4430-4442.
36. Cordero, B.; Gómez, V.; Platero-Prats, A. E.; Revés, M.; Echeverría, J.; Cremades, E.; Barragán, F.; Alvarez, S. "Covalent radii revisited." *Dalton Trans.* **2008**, 2832-2838.
37. Aldridge, S.; Baker, R. J.; Coombs, N. D.; Jones, C.; Rose, R. P.; Rossin, A.; Willock, D. J. "Complexes of a gallium heterocycle with transition metal dicyclopentadienyl and cyclopentadienylcarbonyl fragments, and with a dialkylmanganese compound." *Dalton Trans.* **2006**, 3313-3320.
38. Hickey, A. K.; Chen, C.-H.; Pink, M.; Smith, J. M. "Low-Valent Iron Carbonyl Complexes with a Tripodal Carbene Ligand." *Organometallics* **2015**, *34*, 4560-4566.
39. Hickey, A. K.; Lee, W.-T.; Chen, C.-H; Pink, M.; Smith, J. M. "A Bidentate Carbene Ligand Stabilized a Low-Coordinate Iron(0) Carbonyl Complex." *Organometallics* **2016**, *35*, 3069-3073.\
40. Polezhaev, A. V.; Liss, C. J.; Telser, J.; Chen, C.-H.; Caulton, K. G. "A PNNH Pincer Ligand Allows Access to Monovalent Iron." *Chem. Eur. J.* **2018**, *24*, 1330-1341.
41. (a) Mukhopadhyay, T. K.; Rock, C. L.; Hong, M.; Ashley, D. C.; Groy, T. L.; Baik, M.-H.; Trovitch, R. J. "Mechanistic Investigation of Bis(imino)pyridine Manganese Catalyzed Carbonyl and Carboxylate Hydrosilylation." *J. Am. Chem. Soc.* **2017**, *139*, 4901-4915. (b) Trovitch, R. J. "The Emergence of Manganese-Based Carbonyl Hydrosilylation Catalysts." *Acc. Chem. Res.* **2017**, *50*, 2842-2852.
42. Russell, S. K.; Bowman, A. C.; Lobkovsky, E.; Wieghardt, K.; Chirik, P. J. "Synthesis and Electronic Structure of Reduced Bis(imino)pyridine Manganese Compounds." *Eur. J. Inorg. Chem.* **2012**, 535-545.
43. Weil, J. A.; Bolton, J. R. *Electron Paramagnetic Resonance: Elementary Theory and Practical Applications*; Wiley: Hoboken, NJ, 2007.
44. Stoll, S.; Schweiger, A. "EasySpin, a comprehensive software package for spectral simulation and analysis in EPR." *J. Magn. Reson.* **2006**, *178*, 42-55.
45. Gaussian 09, Revision A.02, Frisch, M. J.; Trucks, G. W.; Schlegel, H. B.; Scuseria, G. E.; Robb, M. A.; Cheeseman, J. R.; Scalmani, G.; Barone, V.; Mennucci, B.; Petersson, G. A.; Nakatsuji, H.; Caricato, M.; Li, X.; Hratchian, H. P.; Izmaylov, A. F.; Bloino, J.; Zheng G.;

Sonnenberg, J. L.; Hada, M.; Ehara, M.; Toyota, K.; Fukuda, R.; Hasegawa, J.; Ishida, M.; Nakajima, T.; Honda, Y.; Kitao, O.; Nakai, H.; Vreven, T.; Montgomery Jr., J. A.; Peralta, J. E.; Ogliaro, F.; Bearpark, M.; Heyd, J. J.; Brothers, E.; Kudin, K. N.; Staroverov, V. N.; Kobayashi, R.; Normand, J.; Raghavachari, K.; Rendell, A.; Burant, J. C.; Iyengar, S. S.; Tomasi, J.; Cossi, M.; Rega, N.; Millam, J. M.; Klene, M.; Knox, J. E.; Cross, J. B.; Bakken, V.; Adamo, C.; Jaramillo, J.; Gomperts, R.; Stratmann, R. E.; Yazyev, O.; Austin, A. J.; Cammi, R.; Pomelli, C.; Ochterski, J. W.; Martin, R. L.; Morokuma, K.; Zakrzewski, V. G.; Voth, G. A.; Salvador, P.; Dannenberg, J. J.; Dapprich, S.; Daniels, A. D.; Farkas, O.; Foresman, J. B.; Ortiz, J. V.; Cioslowski, J.; Fox, D. J. Gaussian, Inc., Wallingford CT, 2009.

46. (a) Perdew, J. P.; Burke, K.; Ernzerhof, M. "Generalized Gradient Approximation Made Simple." *Phys. Rev. Lett.* **1996**, *77,* 3865-3868. (b) Perdew, J. P.; Burke, K.; Ernzerhof, M. "Generalized Gradient Approximation Made Simple." *Phys. Rev. Lett.* **1997**, *78,* 1396.
47. Rassolov, V. A.; Ratner, M. A.; Pople, J. A.; Redfern, P. C.; Curtiss, L. A. "6-31G* Basis Set for Third-Row Atoms." *J. Comp. Chem.* **2001**, *22*, 976-984.
48. (a) Binning Jr., R. C.; Curtiss, L. A. "Compact Contracted Basis Sets for Third-Row Atoms: Ga-Kr." *J. Comp. Chem.* **1990**, *11,* 1206-1216. (b) Curtiss, L. A.; McGrath, M. P.; Blaudeau, J.-P.; Davis, N. E.; Binning Jr., R. C.; Radom, L. "Extension of Gaussian-2 theory to molecules containing third-row atoms Ga-Kr." *J. Chem. Phys.* **1995**, *103,* 6104-6113.
49. Becke, A. D. "Density-functional exchange-energy approximation with correct asymptotic behavior." *Phys. Rev. A* **1998,** *38,* 3098-3100.
50. Becke, A. D. "Density-functional thermochemistry. III. The role of exact exchange." *J. Chem. Phys.* **1993**, *98*, 5648-5652.
51. Lee, C.; Yang, W.; Parr, R. G. "Development of the Colle-Salvetti correlation-energy formula into a functional of the electron density." *Phys. Rev. B* **1988**, *37*, 785−789.
52. Vosko, S. H.; Wilk, L.; Nusair, M. "Accurate spin-dependent electron liquid correlation energies for local spin density calculations: a critical analysis." *Can. J. Phys.***1980**, *58*, 1200-1211.
53. Stephens, P. J.; Devlin, F. J.; Chabalowski, C. F.; Frisch, M. J. "*Ab Initio* Calculation of Vibrational Absorption and Circular Dichroism Spectra Using Density Functional Force Fields." *J. Phys. Chem.* **1994**, *98,* 11623-11627.
54. Chemissian 4.53 (http://www.chemissian.com/).

Table of Contents Graphic

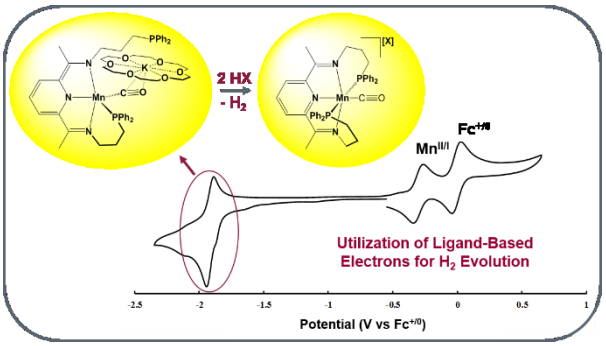

Table of Contents Synopsis

The reduction of [(^{Ph2PPr}PDI)Mn(CO)][Br] has allowed for the preparation of a neutral complex, (^{Ph2PPr}PDI)Mn(CO), and compounds that feature inner-sphere potassium ion coordination including [(κ^4-^{Ph2PPr}PDI)Mn(μ-η^1,η^1,η^2-CO)K(Et_2O)]$_2$, [(κ^4-^{Ph2PPr}PDI)Mn(μ-η^1,η^1-CO)K(MTBE)$_2$]$_2$, and (κ^4-^{Ph2PPr}PDI)Mn(μ-η^1,η^2-CO)K(18-crown-6). Electronic structure analysis revealed that each of these products possess a redox active ^{Ph2PPr}PDI chelate. The addition of non-coordinating acids to (κ^4-^{Ph2PPr}PDI)Mn(μ-η^1,η^2-CO)K(18-crown-6) afforded hydrogen as well as the corresponding Mn(I) compounds, [(^{Ph2PPr}PDI)Mn(CO)][BF_4] and [(^{Ph2PPr}PDI)Mn(CO)][OTf].